Desalination and Water Treatment
www.deswater.com

doi: 10.5004/dwt.2019.23413

142 (2019) 353–363
February

Preparation of Fe(III)-Salen-grafted Fe_3O_4 magnetic composites and their degradation of 2,4,6-trichlorophenol *via* Fenton-like reaction under visible light

Le-Yi Weng, Yu-Fei Wang, Hao-Yu Shen*[,1], Mei-Qin Hu

Ningbo Institute of Technology, Zhejiang University, Ningbo, Zhejiang 315100, China, Tel. +86-574-88130130; emails: hyshen@nit.zju.edu.cn (H.-Y. Shen), 1102325480@qq.com (L.-Y. Weng), 2191983057@qq.com (Y.-F. Wang), mqhu@nit.zju.edu.cn (M.-Q. Hu)

Received 6 May 2018; Accepted 31 October 2018

ABSTRACT

Ethylenediamine (EDA)-functionalized nano-Fe_3O_4 magnetic particle (EDA@nFe_3O_4) was first synthesized by solvothermal method, followed by condensation with 3 kinds of salicylaldehydes, and coordinated with Fe(III) ion to obtain 3 kinds of Fe(III)-Salen (salicylaldehydoethylenediamine)-grafted Fe_3O_4 magnetic composites (nFe_3O_4@Fe(III)Salen). The nFe_3O_4@Fe(III)Salen composites were characterized by elementary analyzer, X-ray diffractometer, FTIR, ultraviolet Vis DRS, XPS, transmission electron microscopy, and vibrating sample magnetometer. The results showed that the nFe_3O_4@Fe(III)Salen composites had an average size of ~200 nm, with the saturation magnetization intensity of 20.3–24.8 emu/g. The nFe_3O_4@Fe(III)Salen can be used as heterogeneous catalyst for the degradation of 2,4,6-trichlorophenol (2,4,6-TCP) *via* Fenton-like reaction under visible light. Radical-trapping experimental results indicated that the •OH radicals were the dominant active oxidizing species in the photoreaction process. The results showed that the highest degradation efficiency to 2,4,6-TCP was found when the nonsubstituted Fe(III)-Salen-grafted composite, nFe_3O_4@Fe(III)Salen, was used as catalyst. Further degradation studies indicated that at pH 4.0–7.0, with the usage amount of nFe_3O_4@Fe(III)Salen above 0.8 g/L and hydrogen peroxide (H_2O_2) concentration at 8.16–40.8 mmol/L, the degradation of 2,4,6-TCP with initial concentration less than 50.0 mg/L (253.2 mg/L) can reach almost 100% under the nFe_3O_4@Fe(III)Salen/H_2O_2/vis system within 5 min, which showed a wider pH range than that of normal Fenton system. nFe_3O_4@Fe(III)Salen can be reused after regeneration for at least 5 times (with degradation percentage of 2,4,6-TCP over 95%). It is a potential effective and reusable material for catalytic degradation of 2,4,6-TCP.

Keywords: Fe(III)-salen-functionalized Fe_3O_4; Magnetic composite; 2,4,6-Trichlorophenol; Degradation; Fenton-like reaction

1. Introduction

Chlorophenols (CPs) are widely used pesticides, disinfectants, wood preservatives, and pulp bleaching agents [1], resulting in the release of CPs into the environment. Because of their high toxicity to aquatic life, persistence, and bioaccumulation potential, some of the CPs, such as 2,4-dichlorophenol, 2,4,6-trichlorophenol (2,4,6-TCP), and pentachlorophenol, have been regulated as priority pollutants by the US Environmental Protection Agency, European Commission (EC) Environmental Directive (2455/2001/EC), and China [2]. Attention has been paid to develop an effective

[1] Dedicated to Prof. Dai-Zheng Liao on the occasion of his 80th birthday.
* Corresponding author.

approach for the treatment of CP-containing wastewater in recent years. Among the potential effective treatment techniques, the development of new adsorbents for effective removal and separation of CPs in environmental matrices is of particular significance.

Some kinds of adsorbents for CP-containing wastewater treatment have been developed, such as activated carbon [3,4], fiber composites [5], resins [6], biochar [7], and molecularly imprinted polymers [8]. Recently, Fe_3O_4-based magnetic nanoparticles (MNPs) have been found to be simple, convenient, and powerful approaches for the separation and purification of environmental samples and removal of toxic pollutants in water [8–14]. Although such MNPs possess unique magnetic properties and can be separated simply from the solution by a magnetic field, how to treat the post-adsorption material is still facing great challenge.

Advanced oxidation processes (AOPs) have been proposed as offering promise for CP pollutant treatment [15–19]. Among AOPs, oxidation using Fenton's reagent is an attractive treatment for the effective degradation of CPs because of its low cost and the lack of toxicity of the reagents [20]. Recently, it has proved that the Fe^{3+} transition metal complex-hydrogen peroxide (H_2O_2) system has the advantages of high utilization rate of H_2O_2 than the conventional Fenton oxidation method [21]. Among them, the metal Schiff-base complex has attracted much attention due to the peculiar electronic characteristics and stable structure and tailoring the electronic and space effect of complex accurately and easily by changing the ligand or metal ion [22]. The iron Schiff-base can act as catalyst in lots of oxidation reactions, which not only overcome the shortcomings of high acidity requirements but also exhibit some characteristics of biomimetic reactions [21]. However, separation and regeneration of the catalyst from the post-run solution is still a problem to be solved. Recently, magnetic materials exhibit high-efficiency photocatalytic degradation properties on environmental pollutants [23].

It would be desirable if three of the promising concepts (high adsorption capacity, magnetic separation, and effective degradation) were combined. Herein, we reported the design and successful synthesis of 3 kinds of Fe(III)-Salen nano-Fe_3O_4 magnetic composite materials (nFe_3O_4@Fe(III)Salen). The nFe_3O_4@Fe(III)Salen were used as heterogeneous catalysts for the degradation of 2,4,6-TCP *via* Fenton-like reaction under visible light. The presumed degradation mechanism was deeply investigated in the present work.

2. Experimental

2.1. Materials

Ferric chloride ($FeCl_3{\cdot}6H_2O$), sodium acetate (NaAc), ethylene glycol (EG), 30% H_2O_2 solution, salicylaldehyde (SA), 4-hydroxy-salicylaldehyde (4-OH-SA), 3-*tert*-butylsalicylaldehyde (3-tBu-SA), *tert*-butanol (tBu-OH), disodium ethylenediamine-tetraacetate (Na_2-EDTA), and benzoquinone were of analytical grade and purchased from Sinopharm Chemical Reagent Co., Ltd. Ethylenediamine (EDA) and 2,4,6-TCP were supplied by Aladdin Chemical Reagent Co., Ltd. (Shanghai, China). LC grade of methanol, acetonitrile, and ammonium acetate (NH_4Ac) were obtained from Merck (Darmstadt, Germany). Distilled water was used to prepare all the solutions. NaOH and HCl solutions of 0.1 mol/L each were used for pH adjustment.

2.2. Preparation of nFe_3O_4@Fe(III)Salen

The overall preparation of EDA-functionalized nano-Fe_3O_4 magnetic composite (EDA@nFe_3O_4) was produced using a polyol-media one-pot solvothermal method according to literature with a minor modification [23]. The 4.0 g of $FeCl_3{\cdot}6H_2O$ and 12.0 g of NaAc were dissolved in 120 mL EG. This solution was stirred vigorously at room temperature for 10 min to form a stable orange solution. A 40 mL of EDA was then added with constant stirring for 30 min until completely dissolved. The mixture solution was then transferred to a Teflon-lined autoclave and heated at 180°C for 8 h. After the autoclave cooled to room temperature, the resulting EDA@nFe_3O_4 was isolated under magnetic field and washed with water and ethanol to remove redundant reagents and impurities. The as-prepared EDA@nFe_3O_4 was dried in a vacuum oven at 60°C for 12 h and stored in a sealed bottle for further use.

A 1.0 g of EDA@nFe_3O_4 was dispersed in 25 mL methanol with ultrasonication for 10 min. A 10 g of SA, 4-OH-SA, or 3-tBu-SA was added under vigorous stirring. The reaction was continued at room temperature for 2 h. The resulting Salen-modified magnetic Fe_3O_4, named as nFe_3O_4@Salen, nFe_3O_4@4-OH-Salen, and nFe_3O_4@3-tBu-Salen, respectively, were collected in a magnetic field, repeatedly washed several times with de-ionized water and ethanol to remove excess salicylaldehyde, and dried under vacuum at 60°C for 12 h. A 0.1 g of nFe_3O_4@Salen was dispersed in 20 mL methanol with ultrasonication for 10 min. A 0.05 g of $FeCl_3{\cdot}6H_2O$ dissolved in another 20 mL methanol was added dropwise under vigorous stirring. The reaction was continued at 65°C for 5 h. The resulting Salen-modified magnetic materials, nFe_3O_4@Fe(III)Salen, nFe_3O_4@Fe(III)4-OH-Salen, or nFe_3O_4@Fe(III)3-tBu-Salen, were collected in a magnetic field, repeatedly washed several times with de-ionized water and ethanol to free of Fe(III) ions, and dried under vacuum at 60°C for 12 h. The overall preparation procedure was shown in Fig. 1.

2.3. Characterization

The morphology and dimensions of the synthesized nFe_3O_4@Fe(III)Salen were examined by transmission electron microscopy (TEM) (Hitachi H-7650) at 80 kV. Each sample was prepared by placing a dilute particle suspension onto 400-mesh carbon grids coated with copper film. Magnetic behavior was analyzed by a vibrating sample magnetometer (VSM) (Lake Shore 7410). The structures of nFe_3O_4@Fe(III)Salen were determined by an X-ray diffractometer (XRD) (Bruker D8 Advance) at ambient temperature. The instrument was equipped with a copper anode generating Cu Ka radiation (λ = 1.5406 Å). FTIR spectra were recorded on a Thermo Nicolet (NEXUS-470) FTIR spectrometer. Ultraviolet (UV)-Vis DRS was recorded on a Perkin Elmer Lambda 950 UV/Vis/NIR spectroscopy. XPS was recorded on an AXIS ULTRADLD X-ray photoelectron

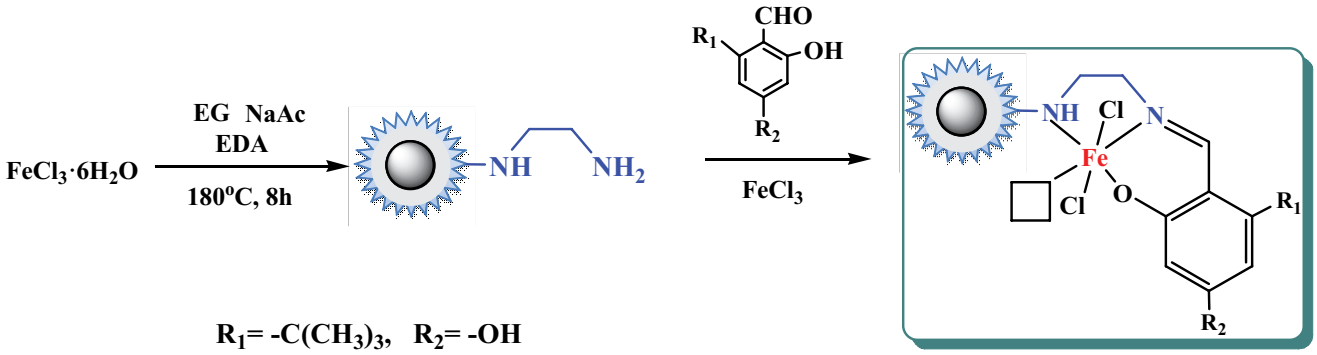

Fig. 1. Synthesis of nFe_3O_4@Fe(III)Salen.

spectroscopy. Thermogravimetry and differential thermogravimetry analyses on a TG 209 F1 instrument at a heating rate of 20°C/min, in a nitrogen atmosphere with a flow rate of 20 mL/min, were carried out. Nitrogen percentage of nFe_3O_4@Fe(III)Salen was analyzed with an elementary analyzer (EA) (ThermoFisher Flash-1112). Fe_3O_4 percentage was calculated *via* the content of the Fe of nFe_3O_4@Fe(III) Salen, which was obtained by detection of iron ions using atomic absorption spectrometry (PE AA 800). The concentration of 2,4,6-TCP in the aqueous solution was analyzed by HPLC method. The HPLC analysis was performed on an Elite HPLC system including a binary pump and a UV detector (Elite Corporation, PRC), using a ZORBAX SB-C8 (5 μm particle size, 250 × 4.6 mm) analytical column. The mobile phase was using a 70:30 methanol and 5 mmol/L NH_4Ac aqueous solution (v/v) at a flow rate of 1.0 mL/min. The analytes were detected by DAD at 230 nm. Column was maintained at a temperature of 35°C to enhance the retention time and reproducibility, and the injection volume was 20.0 μL.

2.4. Catalytic degradation of 2,4,6-TCP by nFe_3O_4@Fe(III)Salen

Catalytic degradation experiments were carried out in 150 mL stoppered flasks, each of which contained 25.00 mL of 2,4,6-TCP solution at concentrations in the range of 0.5–200 mg/L; 20 mg of nFe_3O_4@Fe(III)Salen was added into each flask; 1–100 μL of 30% H_2O_2 was then added. The mixture was shaken at 150 rpm in a thermostatic shaker, sampling at every 1 min, followed by adding 1 drop of 10% Na_2SO_3 solution to stop the reaction. NaOH methanol solution (1%) was used for the desorption of the 2,4,6-TCP on the nFe_3O_4@Fe(III)Salen. HPLC method was applied for the residue 2,4,6-TCP concentrations of both the post-catalytic reaction solution and the desorption solution. The degradation rates of 2,4,6-TCP under different loading amounts and different pH conditions were calculated according to Eq. (1):

$$D = \frac{A_0 - A_t}{A_0} \times 100\% \quad (1)$$

where D is the degradation rate of 2,4,6-TCP; A_t and A_0 are the HPLC peak areas of 2,4,6-TCP at time t and at time 0, respectively.

2.5. Regeneration investigation

Regeneration experiments were carried out with the 2,4,6-TCP postdegradation nFe_3O_4@Fe(III)Salen samples. The postdegradation materials were isolated under magnetic field, and washed with water and ethanol, dried in a vacuum oven at 60°C for 12 h for regeneration investigation. The regeneration experiments were carried out according to the degradation experiments described in 2.4.

3. Results and discussion

3.1. Characterization of nFe_3O_4@Fe(III)Salen

The results of the characterization of 3 kinds of nFe_3O_4@Fe(III)Salen were similar. The main results are listed in Table 1. The characterization of the nFe_3O_4@Fe(III)Salen was taken for detailed discussion as follows.

Table 1
Content of Fe_3O_4 and N and saturation moments of nFe_3O_4@Fe(III)Salen

No.	Composite	Mass fraction of Fe_3O_4/wt%	Mass fraction of N/wt%	TGA		Saturation moments (emu/g)
				T_1/°C (weight loss percentage /%)	T_2/°C (weight loss percentage /%)	
1	nFe_3O_4@Fe(III)Salen	13.28	0.82	417.2 (58.32)	565.8 (13.46)	12.78
2	nFe_3O_4@4-OH-Salen	12.86	0.68	417.8 (59.52)	565.6 (13.58)	12.39
3	nFe_3O_4@Fe(III)3-tBu-Salen	10.78	0.56	417.4 (59.36)	565.2 (13.38)	10.56

The FTIR spectra of EDA@nFe$_3$O$_4$ (Fig. 2(a)), nFe$_3$O$_4$@Salen (Fig. 2(b)), and nFe$_3$O$_4$@Fe(III)Salen (Fig. 2(c)) are shown in Fig. 2. As shown in Fig. 2(a), the characteristic band of Fe–O occurs at 584 cm^{-1} for EDA@Fe$_3$O$_4$. The broad peak appeared at ~3,380 cm^{-1} can be the stretching of the vibration of the –OH group. The characteristic bands of C–H absorption at 2,920, 2,860 cm^{-1} for ν(C–H) of –CH$_2$–,–CH$_3$ groups seems to be incomplete. The characteristic bands at ~1,630 and ~1,550 cm^{-1} can be assigned to be the stretching and bending vibrations of the –NH and –NH$_2$ groups, while the typical band at ~1,060 cm^{-1} can be assigned to be the stretching vibrations of the C–N band of EDA [21]. After condensation with SA to form nFe$_3$O$_4$@Salen, the typical band of –NH$_2$ group at ~1,550 cm^{-1} disappeared and that at ~1,060 cm^{-1} became weaker and shifted to ~1,040 cm^{-1}, shown in Fig. 2(b), indicating the successful formulation of imine group *via* condensation of EDA@nFe$_3$O$_4$ with SA. New peaks at ~1,480, ~1,450, and ~1,230 cm^{-1}, assigned to imine group, benzene ring, and phenolic hydroxyl, respectively, can also be found in Fig. 2(b), further supporting the successful formulation of nFe$_3$O$_4$@Salen [21,23]. After coordination with Fe(III), the typical peak at ~1,480 cm^{-1} disappeared, that at ~1,230 cm^{-1} became weaker and shifted to ~1,250 cm^{-1}, and that at ~1,040 cm^{-1} shifted to ~1,230 cm^{-1}, shown in Fig. 2(c), indicating the successful formulation of nFe$_3$O$_4$@Fe(III)Salen.

The UV-Vis DRS spectra of EDA@nFe$_3$O$_4$ (Fig. 3(a)), nFe$_3$O$_4$@Salen (Fig. 3(b)), and nFe$_3$O$_4$@Fe(III)Salen (Fig. 3(c)) are shown in Fig. 3. As shown in Fig. 3(a), no obvious absorption was observed for EDA@nFe$_3$O$_4$. After formation of Salen grafted to nFe$_3$O$_4$ (Fig. 3(b)), characteristic peaks of π-π* transition and *n*-π* transition absorption of benzene ring and imine appeared below 300 nm [24]. After forming nFe$_3$O$_4$@Fe(III)Salen (Fig. 3(c)), the d-d transition absorption peak of Fe(III) at 518 nm and charge-transfer band of Fe(III)-Salen at 473 nm were observed, implying the successful formation of the composite with potential visible light responsive activity [24].

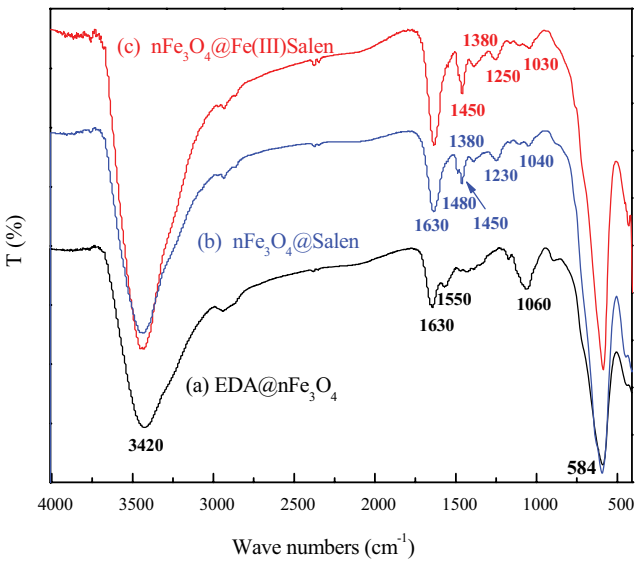

Fig. 2. FTIR of EDA@nFe$_3$O$_4$ (a), nFe$_3$O$_4$@Salen (b), and nFe$_3$O$_4$@Fe(III)Salen (c).

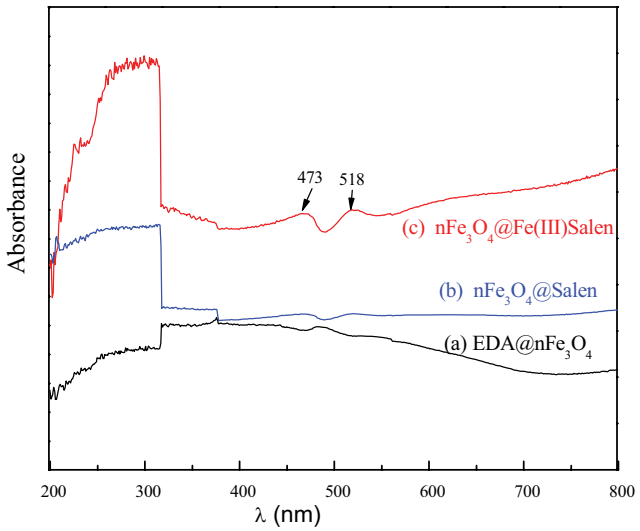

Fig. 3. UV-Vis DRS of EDA@nFe$_3$O$_4$ (a), nFe$_3$O$_4$@Salen (b), and nFe$_3$O$_4$@Fe(III)Salen (c).

The TEM image of EDA@nFe$_3$O$_4$, nFe$_3$O$_4$@Salen, and nFe$_3$O$_4$@Fe(III)Salen are shown in Fig. 4(a)–(c), respectively. It revealed that the nFe$_3$O$_4$@Fe(III)Salen particles were multidispersed with an average diameter of around 200 nm; almost no morphology changed during the process of the condensation and coordination reactions. The XRD patterns of EDA@nFe$_3$O$_4$ (Fig. 5(a)), nFe$_3$O$_4$@Salen (Fig. 5(b)), and nFe$_3$O$_4$@Fe(III)Salen (Fig. 5(c)) are shown in Fig. 5. It indicated that all the three had retained the spinel structure of Fe$_3$O$_4$, in which the identical peaks for Fe$_3$O$_4$ are located at 30.1°, 35.5°, 43.1°, 53.4°, 57.0°, and 62.6°, corresponding to their indices (220), (311), (400), (422), (511), and (400) [8]. The intensity of diffraction peaks of nFe$_3$O$_4$@Fe(III)Salen became slightly broader than that of pure Fe$_3$O$_4$, indicating a small scale of nFe$_3$O$_4$@Fe(III)Salen is expected.

EA results showed that the elemental percentage of nFe$_3$O$_4$@Fe(III)Salen was at C: 58.34%, H: 7.12%, N: 0.82%, and O: 20.45%, while the total content of Fe$_3$O$_4$ in the nFe$_3$O$_4$@Fe(III)Salen was 13.28%. The nitrogen content of the substituted nFe$_3$O$_4$@Fe(III)Salen decreased from 0.82% to 0.68% and 0.56% when 4-OH-SA and 3-tBu-SA were used for condensation. The TG/DTG analysis of nFe$_3$O$_4$@Fe(III)Salen is shown in Fig. 6. Two weight losses at around ~417°C (58.32%–59.36%) and ~565°C (13.46%–13.58%) for all the 3 kinds of nFe$_3$O$_4$@Fe(III)Salen were found, which could be attributed to the desorption of the functional groups anchored on the surface.

The surface area measured by BET (S_{BET}) of nFe$_3$O$_4$@Fe(III)Salen was measured to be 0.09 m^2/g, which indicated that nFe$_3$O$_4$@Fe(III)Salen were nonporous.

The paramagnetic property of the nFe$_3$O$_4$@Fe(III)Salen was verified by the magnetization curve measured by VSM, shown in Fig. 7. The saturation moment obtained from the hysteresis loop was found to be 24.8 emu/g. Similar results were obtained for nFe$_3$O$_4$@Fe(III)4-OH-Salen and nFe$_3$O$_4$@Fe(III)3-tBu-Salen with the saturation moments at 21.2 emu/g and 20.3 emu/g, respectively. All the 3 kinds of nFe$_3$O$_4$@Fe(III)Salen were expected to respond well to magnetic fields without any permanent magnetization, therefore making the solid and liquid phases separate easily.

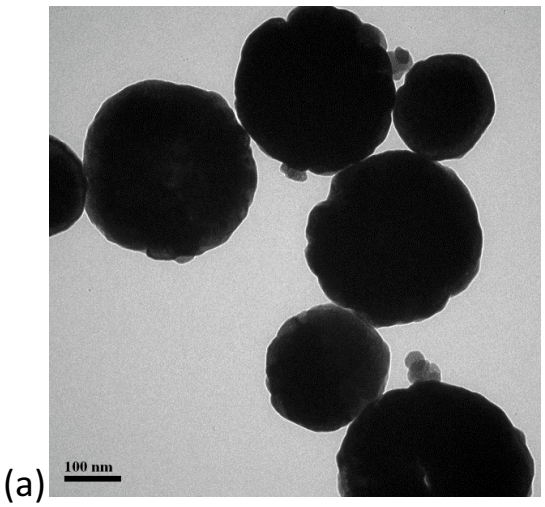

Fig. 4. TEM of EDA@nFe_3O_4 (a), nFe_3O_4@Salen (b), and nFe_3O_4@ Fe(III)Salen (c).

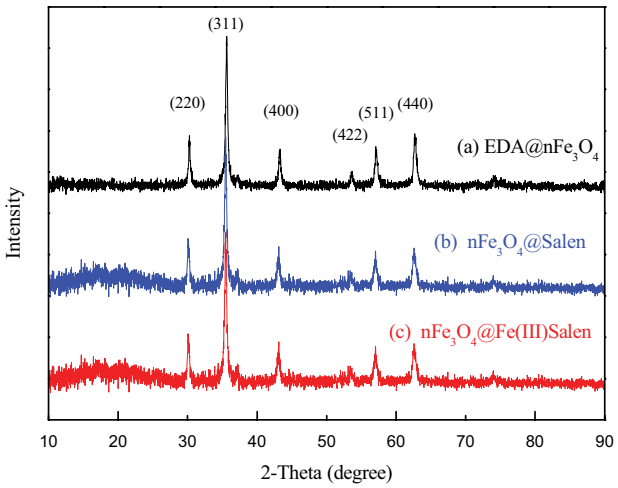

Fig. 5. XRD of EDA@nFe_3O_4 (a), nFe_3O_4@Salen (b), and nFe_3O_4@ Fe(III)Salen (c).

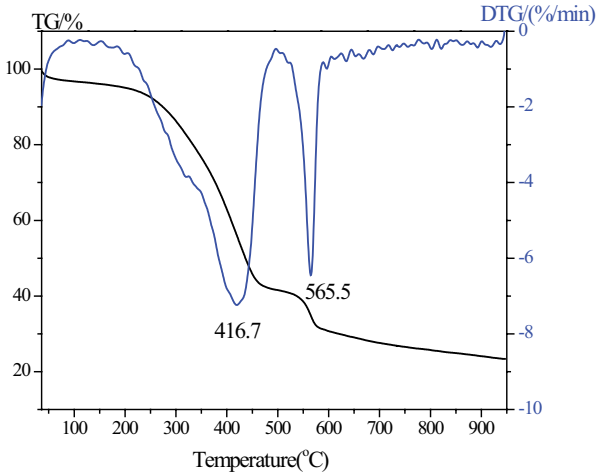

Fig. 6. TG-DTG curves of the nFe_3O_4@Fe(III)Salen.

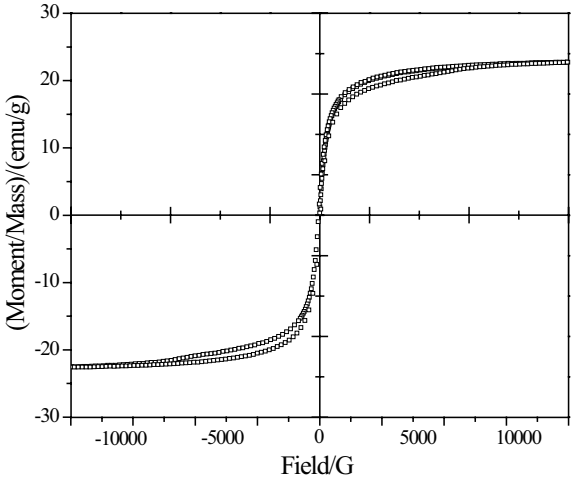

Fig. 7. VSM of the nFe_3O_4@Fe(III)Salen.

3.2. Degradation of 2,4,6-TCP by nFe_3O_4@Fe(III)Salen

3.2.1. Effect of solution pH values on the degradation performance

The effect of solution pH was investigated with the pH values ranging from 3.0 to 9.0, with the initial concentration of 2,4,6-TCP at 50 mg/L, and the results are shown in Fig. 8. The catalytic degradation rate of 2,4,6-TCP was dependent on solution pH. With the solution pH increasing, the degradation rate first increased with the solution pH < 4.0 and reached a plateau value with pH ranging from 4.0 to 7.0 and then decreased at the pH > 7.0 Overall, the nFe_3O_4@Fe(III) Salen/H_2O_2/vis catalytic system has a much wider pH range than that of common Fenton reaction system [15]. This might be due to the fact that Fe(III) coordinated with Salen in the nFe_3O_4@Fe(III)Salen to form a Fenton-like heterogeneous catalytic system, thus weakening the pH influence on catalytic degradation reaction. Under acidic conditions (pH < 4.0), the amino groups on the surface of nFe_3O_4@Fe(III)Salen are easy to be protonated and the main formation was $–NH_2^+$–or –C=NH^+ without lone pair electrons, which are unfavorable to stabilize the Fe(III)-Salen coordination center, leading to a low degradation rate of around 80%. At pH ranging from 4.0 to 7.0, the main formation of the surface groups might be –NH– and –C=N, favorable for the stabilization of the Fe(III)-Salen coordination center. –OH group of 2,4,6-TCP can coordinate to the Fe(III)-Salen active center, and π–π interaction between the benzene rings of 2,4,6-TCP and Salen might also occur, leading to a high adsorptive capacity of 2,4,6-TCP on the surface of nFe_3O_4@Fe(III)Salen. After adding H_2O_2, hydrogen bonds are formed between the –OH group of 2,4,6-TCP and H_2O_2 and •OH released. The catalytic degradation of 2,4,6-TCP was realized *via* a Fenton-like heterogeneous catalytic system, with almost 100% degradation rate of around 80%. When pH > 7.0, OH^- ions may react with the Fe(III) of nFe_3O_4@Fe(III)Salen, leading to deactivation of the catalyst as well as not favorable to the formation of •OH free radicals [21]. Thus, it would be very difficult to realize the Fenton-like reactions, leading to a very low degradation rate (~57%, pH = 8.0; ~42%, pH = 9.0). The presumed degradation mechanism is shown in Fig. 9.

The same procedure of degradation studies was carried out in de-ion water at pH 2.5 (Blank sample). The residue concentration of the iron ions in the posttreatment water was tested by atomic absorption spectrometry (PE AA 800).

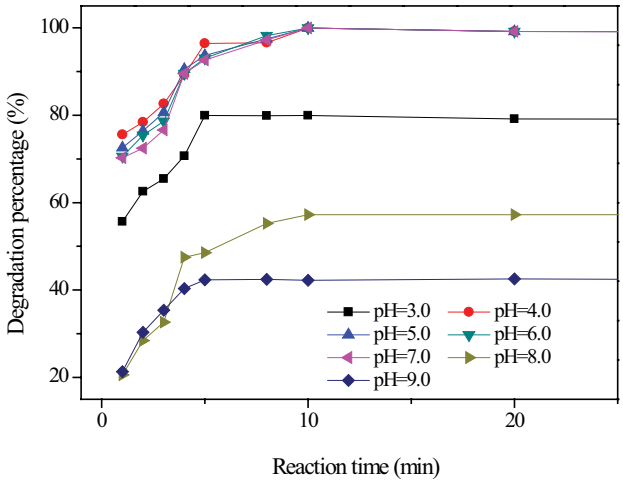

Fig. 8. Effect of the solution pH on the nFe_3O_4@Fe(III)Salen/H_2O_2/Vis-TCP catalytic degradation system.

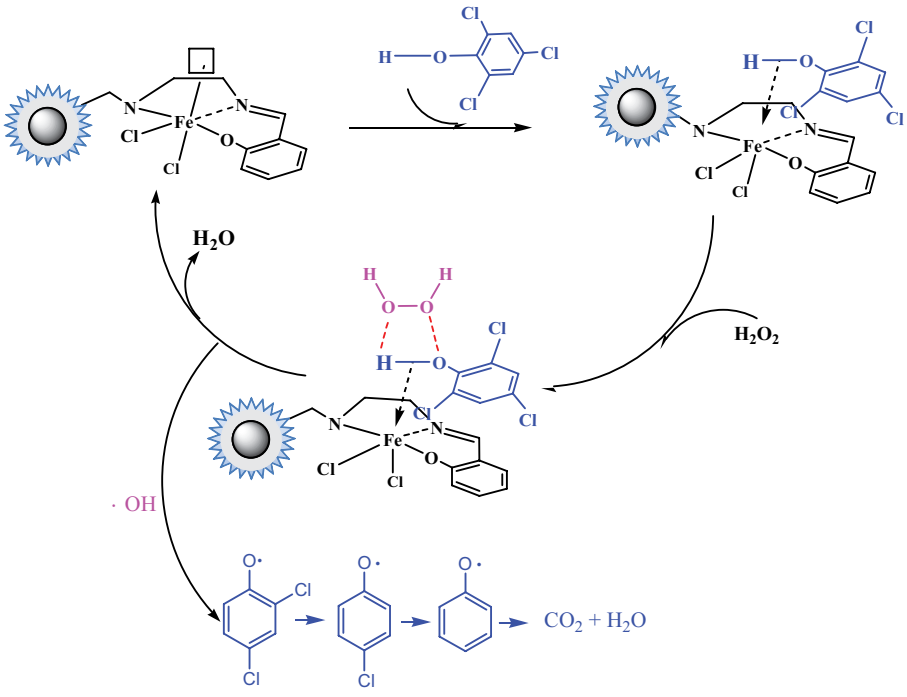

Fig. 9. Presumed mechanism of the nFe_3O_4@Fe(III)Salen/H_2O_2/Vis system for catalytic degradation of TCP.

The results showed that it is free from iron ions in the posttreatment water. The Fe_3O_4 was fully covered, and the functional Fe(III)-Salen center was also stable during degradation studies at low pH.

3.2.2. Effect of usage amount of H_2O_2 on the degradation performance

The effect of usage amount of H_2O_2 was investigated with the volume of 30% H_2O_2 ranging from 0 to 100 μL, i.e., the concentration of H_2O_2 in the catalytic system was in the range of 0.408–40.8 mmol/L, with the initial concentration of 2,4,6-TCP at 50 mg/L. The results are shown in Fig. 10. Without adding H_2O_2, almost no degradation of TCP was observed, which means H_2O_2 is indispensable in the present catalytic system. When the concentration of H_2O_2 was at 0.408–0.816 mmol/L, 40 min were needed for total degradation of TCP. When the concentration of H_2O_2 is at 8.16 mmol/L, 20 min for degradation were needed. With the concentration of H_2O_2 increasing, the degradation rate increased gradually, and only 5 min were needed for total degradation of TCP eventually. No decrease of degradation rate was observed as reported in literature [22]. Normally, the strong degradation ability OH free radicals will transfer to weak degradation ability •OH free radicals when H_2O_2 is at high concentration, as shown in Eq. (2), which is not favorable to the photocatalytic degradation. These results might be owned by the fact that nFe_3O_4@Fe(III)Salen coordination center can make stable •OH free radicals as well as the degradation reactions were carried out in visible light but not the UV light irritation.

$$H_2O_2 + \bullet OH \xrightarrow{hv} H_2O + \bullet OOH \quad (2)$$

The adsorption mechanism could be confirmed by XPS analyses of nFe_3O_4@Fe(III)Salen before and after 2,4,6-TCP adsorption (nFe_3O_4@Fe(III)Salen-A) and degradation (nFe_3O_4@Fe(III)Salen-D), shown in Fig. 11. From the survey scan of XPS spectra (Fig. 11(a)), a new peak owing to Cl2p could be observed after 2,4,6-TCP loaded on to nFe_3O_4@Fe(III)Salen, indicating the successful adsorption of 2,4,6-TCP, while after adding H_2O_2, the peak disappeared, with the degradation of the 2,4,6-TCP, implying the degradation of 2,4,6-TCP followed by adsorption with the aid of H_2O_2. The N1s high-resolution scan of nFe_3O_4@Fe(III)Salen could be deconvoluted into two individual peaks at binding energies of 398.8 and 396.2 eV (Fig. 11(b)), which were assigned to the N atoms in the C–N and the imine groups of Salen [25], respectively. A new peak at 399.6 eV was observed after 2,4,6-TCP adsorption, which could be attributed to the hydrogen bonding of ph-O–H ··· NH_2 or –N–H ··· O-ph [26]. Similarly, these peaks disappeared after the catalytic degradation of 2,4,6-TCP. In the XPS spectra of C1s (Fig. 11(c)), the carbon atoms can be found in two chemically different positions, leading to two differing C1 binding energies: C–C (~283.9 eV) and C–N (~286.5 eV). After adsorption, only one peak at ~284.0 eV with a broader band range appeared, which may attribute to the involvement of the imine groups of Salen in the adsorption of 2,4,6-TCP. Similar phenomena were observed in the XPS spectra of O1s (Fig. 11(d)), the peaks of O1s appeared at ~530.45 eV, assigned to C–O–C and C–OH groups, broadening with a slight shift of binding energies after adsorption of 2,4,6-TCP. After degradation of TCP, these peaks in the high-resolution scan of nFe_3O_4@Fe(III)Salen recovered to those obtained prior to adsorption.

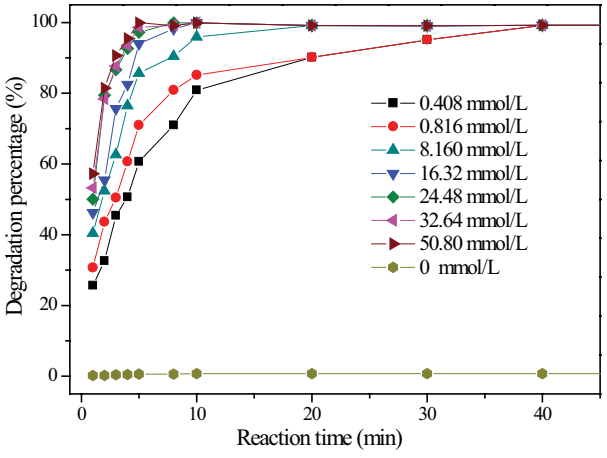

Fig. 10. Effect of the usage amount of H_2O_2 on the nFe_3O_4@Fe(III) Salen/H_2O_2/Vis-TCP catalytic degradation system.

3.2.3. Effect of usage amount of nFe_3O_4@Fe(III)Salen on the degradation performance

The effect of usage amount of nFe_3O_4@Fe(III)Salen was investigated from 10 to 100 mg, i.e., the concentration of nFe_3O_4@Fe(III)Salen in the catalytic system was at 0.4–4.0 g/L, with the volume of 30% H_2O_2 at 30 μL, and the initial concentration of 2,4,6-TCP at 50 mg/L. The results are shown in Fig. 12. nFe_3O_4@Fe(III)Salen was the key factor for the generation of the •OH free radicals. When the usage amount of nFe_3O_4@Fe(III)Salen was low, the degradation rate of 2,4,6-TCP was very low. With the usage amount of nFe_3O_4@Fe(III) Salen increases, the generation rate of the •OH free radicals increased, leading to a increase of degradation rate of 2,4,6-TCP. When the usage amount of nFe_3O_4@Fe(III)Salen reached 0.8 g/L, the degradation rate tends to be stable.

3.2.4. Effect of the initial concentration of TCP on the degradation performance

The effect of initial concentration of TCP was investigated from 0.5 to 100 mg/L, i.e., the concentration of TCP in the catalytic system was at 2.53–506.3 mmol/L, with the usage amount of nFe_3O_4@Fe(III)Salen at 0.02 g (i.e., 0.8 g/L in the catalytic system) and the volume of 30% H_2O_2 at 20 μL (i.e., 8.16 mmol/L in the catalytic system). The results are shown in Fig. 13. The results showed that the lower the concentration of TCP, the higher the degradation rate of 2,4,6-TCP. When the concentration of TCP <253.2 mmol/L (50 mg/L), the TCP can be totally investigated. The residue concentration of TCP was at micrograms per liter level in the aqueous environment; thus, the present nFe_3O_4@Fe(III) Salen/H_2O_2/vis system can be used for the treatment of TCP in the environment.

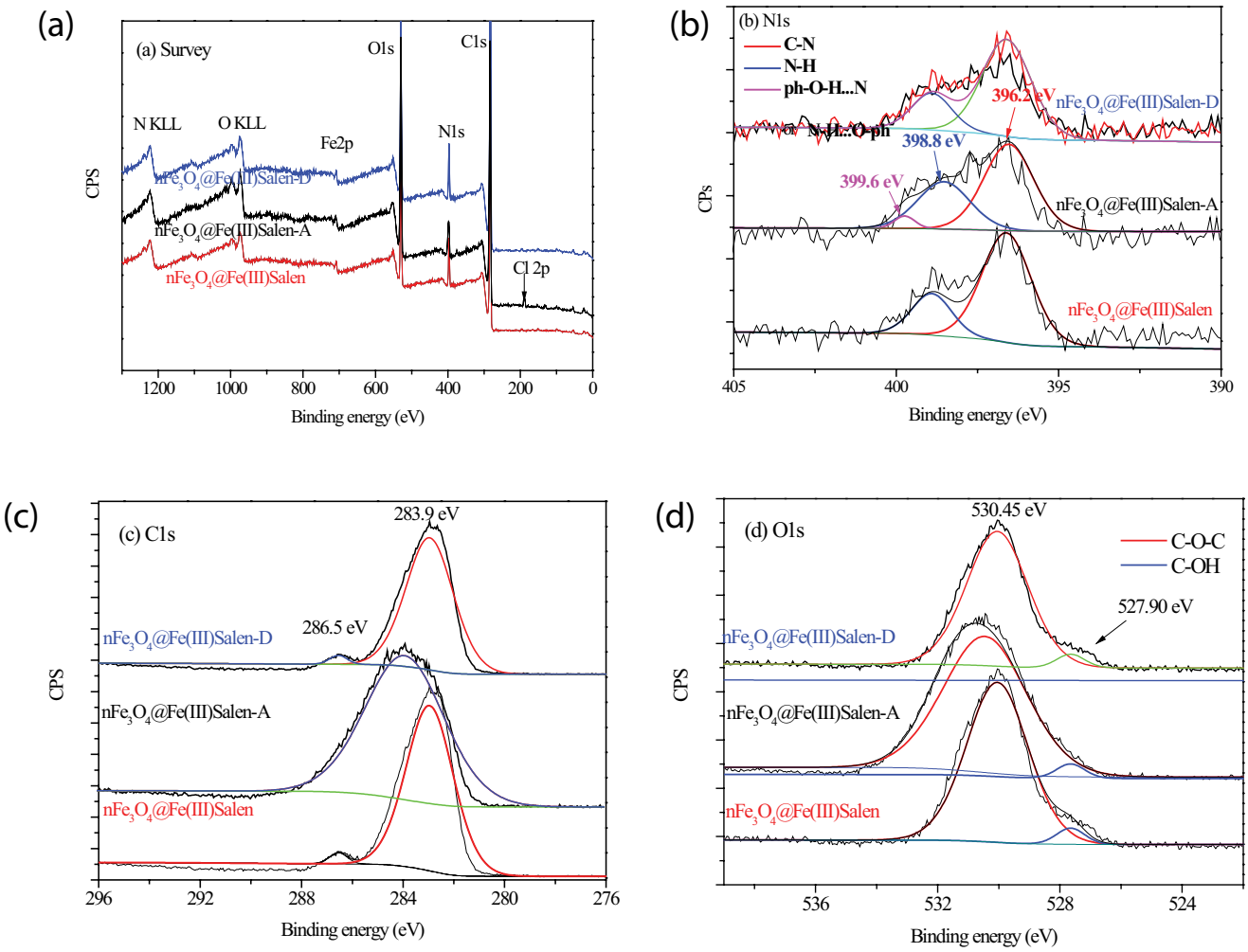

Fig. 11. XPS spectra of (a) survey scan and high-resolution scan of (b) N1s, (c) C1s, and (d) O1s of nFe_3O_4@Fe(III)Salen and after adsorption (nFe_3O_4@Fe(III)Salen-A) and degradation (nFe_3O_4@Fe(III)Salen-D) of TCP.

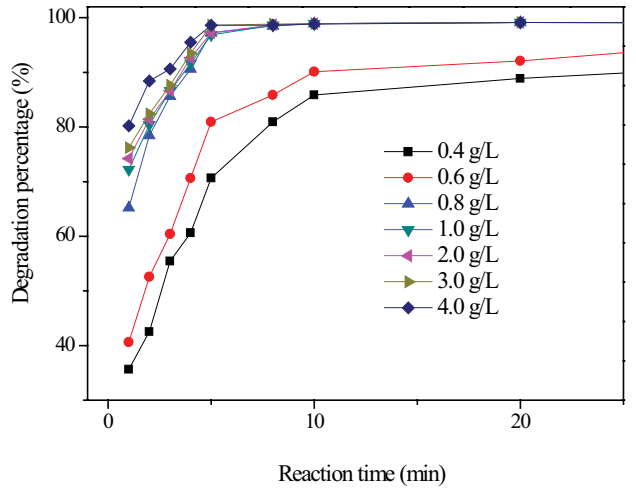

Fig. 12. Effect of the usage amount of nFe_3O_4@Fe(III)Salen on the nFe_3O_4@Fe(III)Salen/H_2O_2/Vis-TCP catalytic degradation system.

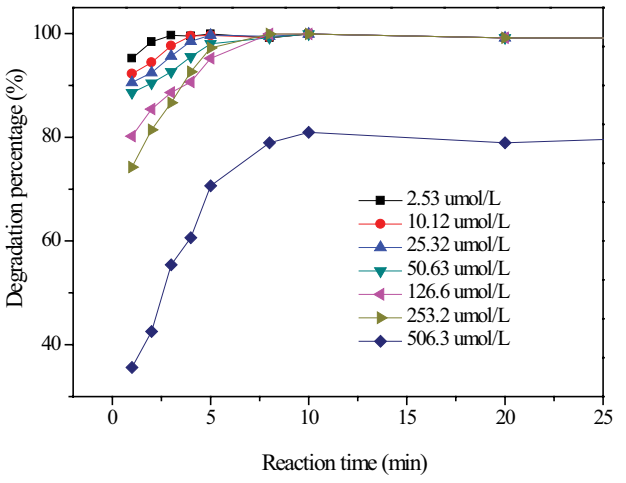

Fig. 13. Effect of the initial concentration of TCP on the nFe_3O_4@Fe(III)Salen/H_2O_2/Vis-TCP catalytic degradation system.

3.3. Reusability investigation

The reusability of the nFe_3O_4@Fe(III)Salen was evaluated by comparing the degradation efficiency. The postdegraded nFe_3O_4@Fe(III)Salen was isolated by magnet, washed with D.I. water for 3 times, dried in a vacuum oven at 60°C for 12 h, and stored in a sealed bottle for another degradation of 2,4,6-TCP. The results for those of the initial concentration of 2,4,6-TCP at 50.0 mg/L are shown in Fig. 14. The results indicated that nFe_3O_4@Fe(III)Salen could be used for at least 5 cycles with a degradation rate higher than 95% upon recovery on average. No obvious decrease in the degradation efficiency was found.

3.4. Radical-trapping experiences

In order to identify the major active species in the photodegradation process, radical-trapping measurements were also performed, according to literature reports [27–30]. The results are displayed in Fig. 15. The photodegradation of 2,4,6-TCP was greatly inhibited (from 97.8% to 3.8%) by the addition of 1 mmol/L tBu-OH (a hydroxyl radical scavenger) for 90 min, indicating that the •OH radicals are the dominant active oxidizing species in the photoreaction process, while the 2,4,6-TCP degradation was slightly inhibited with the use of 1 mmol/L of Na_2-EDTA (a hole scavenger) and benzoquinone (a superoxide anion radical scavenger, $O_2^{\bullet-}$). Therefore, the photogenerated holes and $O_2^{\bullet-}$ are the minor reactive species contributing to the oxidative degradation of 2,4,6-TCP.

3.5. Degradation efficiency comparison

The degradation efficiency to 2,4,6-TCP of the present studied 3 kinds of nFe_3O_4@Fe(III)Salen was compared. The results are listed in Table 2. The results showed that the highest degradation efficiency to 2,4,6-TCP was found

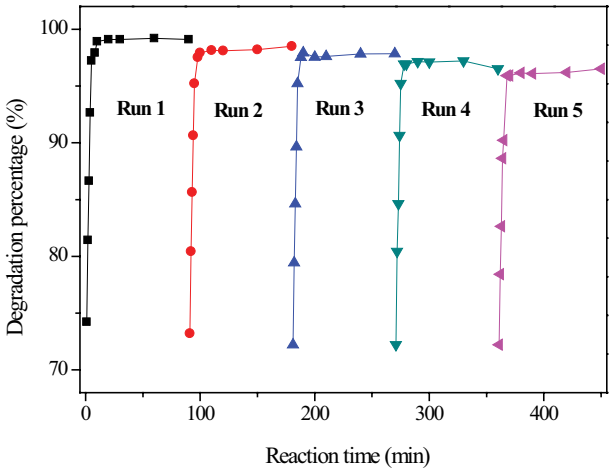

Fig. 14. Recycle of the nFe_3O_4@Fe(III)Salen catalyst.

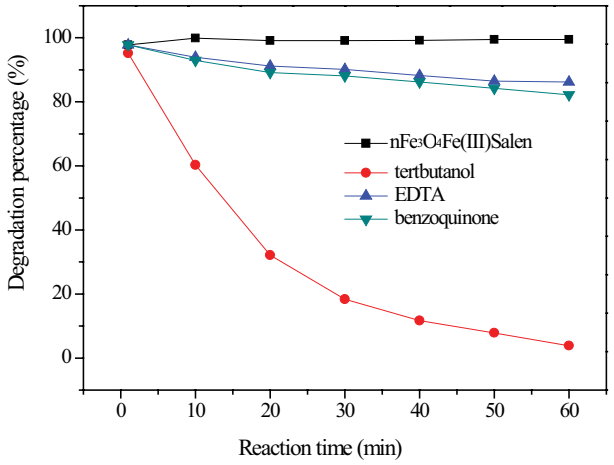

Fig. 15. Plots of active species trapped in the system for the photodegradation of 2,4,6-TCP using nFe_3O_4@Fe(III)Salen catalyst.

Table 2
Comparison of degradation efficiency of nFe_3O_4@Fe(III)Salen to 2,4,6-TCP

No.	Catalyst	Usage amount (g/L)	Initial concentration of TCP (mg/L)	Usage amount of H_2O_2 (mmol/L)	Degradation percentage (%)
1	nFe_3O_4@Fe(III)Salen	0.8	50	8.16	99.2
		4.0	50	8.16	99.8
		0.8	5	8.16	99.9
		0.8	50	40.8	99.4
2	nFe_3O_4@4-OH-Salen	0.8	50	8.16	82.5
		4.0	50	8.16	90.2
		0.8	5	8.16	95.5
		0.8	50	40.8	85.2
3	nFe_3O_4@Fe(III)3-tBu-Salen	0.8	50	8.16	73.2
		4.0	50	8.16	85.6
		0.8	5	8.16	90.6
		0.8	50	40.8	75.6

when the nonsubstituted-Fe(III)-Salen-grafted composite, nFe_3O_4@Fe(III)Salen, was used as catalyst. Although by decreasing the initial concentration of TCP and by increasing the usage amount of the substituted nFe_3O_4@Fe(III)Salen, the degradation efficiency can increase about 10%–15% for nFe_3O_4@4-OH-Salen and nFe_3O_4@Fe(III)3-tBu-Salen; the degradation percentage of nFe_3O_4@Fe(III)Salen was still the highest one. There was only about 3% of the degradation efficiency increased when the usage amount of H_2O_2 was from 8.16 to 40.8 mmol/L for nFe_3O_4@4-OH-Salen and nFe_3O_4@Fe(III)3-tBu-Salen.

4. Conclusion

In this work, 3 kinds of Fe(III)-Salen-grafted Fe_3O_4 composites (nFe_3O_4@Fe(III)Salen) were designed, prepared, and characterized. They were used as catalysts for the Fenton-like reaction of the catalytic degradation of 2,4,6-TCP. The highest degradation efficiency to 2,4,6-TCP was found when the nonsubstituted-Fe(III)-Salen-grafted composite, nFe_3O_4@Fe(III)Salen, was used as catalyst. It is found that in the nFe_3O_4@Fe(III)Salen/H_2O_2/visible light system, the –OH group of TCP can coordinate to the Fe(III) of the nFe_3O_4@Fe(III)Salen activity center and the benzene ring of the TCP can also combine to the Salen *via* π–π interactions, which is favorable to the adsorption of TCP on the surface of the nFe_3O_4@Fe(III)Salen; after adding H_2O_2, the –OH group of TCP can form hydrogen bonds with H_2O_2, followed by further generation of the formation of •OH; thus, *in situ* catalytic degradation of TCP by Fenton-like reaction can be realized. In the range of pH value at 4.0–7.0, nearly 100% degradation of TCP can be realized by the nFe_3O_4@Fe(III)Salen/H_2O_2/visible light system in 5 min. Compared with ordinary Fenton reaction system, a wide range of pH value for the degradation of TCP was achieved. The degradation rate of TCP can reach more than 99% when the usage amount of nFe_3O_4@Fe(III)Salen was at 0.8–4.0 mg/L, the concentration of H_2O_2 at 8.16 mmol/L, and the concentration of 2,4,6-TCP at <253.2 mmol/L (50 mg/L). The nFe_3O_4@Fe(III)Salen could be used for at least 5 cycles with degradation rate higher than 95% upon recovery on average. It is a potential effective and reusable catalyst for the degradation of 2,4,6-TCP.

Acknowledgements

We would like to thank the National Natural Science Foundation of China (51608479, 81502421). We would like to thank the National Natural Science Foundation of Zhejiang Province (LY14B04003), the National Natural Science Foundation of Ningbo (2018A610206), the National College Students' innovation and entrepreneurship training program (201713022009), the Xinmiao Students' innovation training program of Zhejiang Province (2017R401181) for the financial support.

References

[1] G. Cagnetta, J. Robertson, J. Huang, K.L. Zhang, G. Yu, Mechanochemical destruction of alogenated organic pollutants: a critical review, J. Hazard. Mater., 313 (2016) 85–102.
[2] J.Q. Guo, C.H. Wu, S.L. Lv, D.S. Lu, C. Feng, X.J. Qi, W.J. Liang, X.L. Chang, H. Xu, G.Q. Wang, Z.J. Zhou, Associations of prenatal exposure to five chlorophenols with adverse birth outcomes, Environ. Pollut., 214 (2016) 478–484.
[3] J.L. Fan, J. Zhang, C.L. Zhang, L. Reb, Q.Q. Shi, Adsorption of 2,4,6-trichlorophenol from aqueous solution onto activated carbon derived from loosestrife, Desalination, 267 (2011) 139–146.
[4] P. Strachowski, M. Bystrzejewski, Comparative studies of sorption of phenolic compounds onto carbon-encapsulated iron nanoparticles, carbon nanotubes and activated carbon, Colloids Surf., A., 467 (2015) 113–123.
[5] M.M. Machawe, M.T. Justice, A.M.M. Titus, B.M. Bhekie, Adsorption of 2,4,6-trichlorophenol and ortho-nitrophenol from aqueous media using surfactant-modified clinoptilolite-polypropylene hollow fibre composites, Water Air Soil Pollut., 223 (2012) 1555–1569.
[6] M.S. Bilgili, Adsorption of 4-chlorophenol from aqueous solutions by xad-4 resin: isotherm, kinetic, and thermodynamic analysis, J. Hazard. Mater., 137 (2006) 157–164.
[7] S. Mubari, A. Saeed, M.M. Athar, M. Iqbal, Characterization and mechanism of the adsorptive removal of 2,4,6-trichlorophenol by biochar prepared from sugarcane baggase, J. Ind. Eng. Chem., 33 (2016) 115–121.
[8] H.Y. Shen, Z.X. Chen, Z.H. Li, M.Q. Hu, X.Y. Dong, Q.H. Xia, Controlled synthesis of 2,4,6-trichlorophenol-imprinted amino-functionalized nano-Fe_3O_4-polymer magnetic composite for highly selective adsorption, Colloids Surf. A Physicochem. Eng. Asp., 481 (2015) 439–450
[9] C.M. Su. Environmental implications and applications of engineered nanoscale magnetite and its hybrid nanocomposites: a review of recent literature, J. Hazard. Mater., 322 (2017) 48–84.
[10] Y.G. Zhao, X.H. Chen, S.D. Pan, H. Zhu, H.Y. Shen, M.C. Jin, Self-assembly of surface bisphenol A-imprinted core-shell nanoring amino-functionalized superparamagnetic polymer, J. Mater. Chem. A., 1 (2013) 11648–11658.
[11] H.Y. Shen, S.D. Pan, Y. Zhang, X.L. Huang, H.X. Gong, A new insight on the adsorption mechanism of amino-functionalized nano-Fe_3O_4 magnetic polymers in Cu(II), Cr(VI) co-existing water system, Chem. Eng. J., 183 (2012) 180–191.
[12] H.Y. Shen, J.L. Chen, H.F. Dai, L.B. Wang, M.Q. Hu, Q.H. Xia, New insights into the sorption and detoxification of chromium (VI) by tetraethylenepentamine functionalized nano-sized magnetic polymer adsorbents: mechanism and pH effect, Ind. Eng. Chem. Res., 52 (2013) 12723–12732.
[13] S.D. Pan, H.Y. Shen, Q.H. Xu, J. Luo, M.Q. Hu, Surface mercapto engineered magnetic Fe_3O_4 nanoadsorbent for the removal of mercury from aqueous solutions, J. Colloid Interface Sci., 365 (2012) 204–212.
[14] S.D. Pan, Y. Zhang, H.Y. Shen, M.Q. Hu, An intensive study on the magnetic effect of mercapto-functionalized nano magnetic Fe_3O_4 polymers and their adsorption mechanism for the removal of Hg(II) from aqueous solution, Chem. Eng. J., 210 (2012) 564–574.
[15] N.S. Goldstein, D. Meyerstein, Comments on the mechanism of the "Fenton-like" reaction, Acc. Chem. Res., 32 (1999) 547–549.
[16] S.Y. Dong, X.H. Ding, T. Guo, X.P. Yue, X. Han, J.H. Sun, Self-assembled hollow sphere shaped Bi_2WO_6/RGO composites for efficient sunlight-driven photocatalytic degradation of organic pollutants, Chem. Eng. J., 316 (2017) 778–789.
[17] S.Y. Dong, L.J. Xia, T. Guo, F.Y. Zhang, L.F. Cui, X.F. Su, D. Wang, W. Guo, J.H. Sun, Controlled synthesis of flexible graphene aerogels macroscopic monolith as versatile agents for wastewater treatment, Appl. Surf. Sci., 445 (2018) 30–38.
[18] S.Y. Dong, Y.R. Cui, Y.F. Wang, Y.K. Li, L.M. Hu, J.Y. Sun, J.H. Sun, Designing three-dimensional acicular sheaf shaped $BiVO_4$/reduced graphene oxide composites for efficient sunlight-driven photocatalytic degradation of dye wastewater, Chem. Eng. J., 249 (2014) 102–110.
[19] C.F. Yu, K. Wang, P.Y. Yang, S.N. Yang, C. Lu, Y.Z. Song, S.Y. Dong, J.Y. Su, J.H. Sun, One-pot facile synthesis of Bi_2S_3/SnS_2/Bi_2O_3 ternary heterojunction as advanced double Z-scheme photocatalytic system for efficient dye removal under sunlight irradiation, Appl. Surf. Sci., 420 (2017) 233–242.

[20] E. Nevens, J. Baevenes, A review of classic Fenton's peroxidation as an advanced oxidation technique, J. Hazard. Mater. B, 98 (2003) 33–50.
[21] J. Yang, S.Y. Xie, Y. Chen, Synthesis of homogeneous m-H_2O-Fe(III) catalyst and its application in degradation of dibutyl phthalate (DBP), Environ. Chem., 33 (2014) 1930–1935.
[22] L.M. Jiao, X. Huang, X.P. Liao, Catalytic degradation of dimethyl phthalate by photo-assisted Fe(III) immobilized collagen fiber, J. Chem. Ind. Eng., 69 (2011) 3419–3427.
[23] Z.K. Jin, W.J. Dong, M. Yang, J.J. Wang, H.Y. Gao, G. Wang, One-pot preparation of hierarchical nanosheet-constructed Fe_3O_4/MIL-88B(Fe) magnetic microspheres with high efficiency photocatalytic degradation of dye, Chem. Cat. Chem., 8 (2016) 3510–3517.
[24] P. Michorczyk, J. Ogonowski, In situ UV-Vis DRS evidence of Cr^{2+} species oxidation by CO_2, Chem. Commun., 48 (2012) 7283–7285.
[25] Y. Zhang, S.D. Pan, H.Y. Shen, M.Q. Hu, Amino-functionalized nano-size composite materials for dispersive solid phase extraction of phosphate in water samples, Anal. Sci., 28 (2012) 887–892.
[26] M.Q. Hu, H.Y. Shen, Z.H. Jiang, Y.F. Wang, L.Y. Weng, Q. Jiang, One-pot solvothermal preparation of ethylenediamine-functionalized nanochain and its adsorption-in situ degradation of 2,4,6-trichlorophenol, Desal. Wat. Treat., 102 (2018) 253–263.
[27] X.H. Gao, H.B. Wu, L.X. Zheng, Y.J. Zhong, Y. Hu, X.W. Lou, Formation of mesoporous heterostructured $BiVO_4/Bi_2S_3$ hollow discoids with enhanced photoactivity, Angew. Chem. Int. Ed., 53 (2014) 5917–5921.
[28] R. Qiao, M.M. Mao, E.L. Hu, Y.J. Zhong, J.Q. Ning, Y. Hu, Facile formation of mesoporous $BiVO_4$/Ag/AgCl heterostructured microspheres with enhanced visible-light photoactivity, Inorg. Chem., 54 (2015) 9033–9039.
[29] S.L. Wang, J.J. Li, X.D. Zhou, C.C. Zheng, J.Q. Ning, Y.J. Zhong, Y. Hu, Facile preparation of 2D sandwich-like CdS nanoparticles/nitrogen-doped reduced graphene oxide hybrid nanosheets with enhanced photoelectrochemical properties, J. Mater. Chem. A., 2 (2014) 19815–19821.
[30] A. Etogo, E.L. Hu, C.M. Zhou, Y.J. Zhong, Y. Hu, Z.L. Hong, Facile fabrication of mesoporous $BiOCl/(BiO)_2CO_3/Bi_2O_3$ ternary flower-like heterostructured microspheres with high visible-light-driven photoactivity, J. Mater. Chem. A., 3 (2015) 22413–22420.